Biosensors and Bioelectronics 123 (2019) 77–84

Contents lists available at ScienceDirect

Biosensors and Bioelectronics

journal homepage: www.elsevier.com/locate/bios

A bio-inspired 3D micro-structure for graphene-based bacteria sensing

Bing Li, Haijie Tan, Salzitsa Anastasova, Maura Power, Florent Seichepine, Guang-Zhong Yang*

The Hamlyn Centre, Imperial College London, South Kensington, London SW7 2AZ, UK

ARTICLE INFO

Keywords:
Graphene
Label-free bacteria sensing
3D printing
Microfabrication
Bio-inspired device

ABSTRACT

Nature is a great source of inspiration for the development of solutions for biomedical problems. We present a novel biosensor design utilizing two-photon polymerisation and graphene to fabricate an enhanced biosensing platform for the detection of motile bacteria. A cage comprising venous valve-inspired directional micro-structure is fabricated around graphene-based sensing electronics. The asymmetric 3D micro-structure promotes motile cells to swim from outside the cage towards the inner-most chamber, resulting in concentrated bacteria surrounding the central sensing region, thus enhancing the sensing signal. The concentrating effect is proved across a range of cell cultures - from 10^1 CFU/ml to 10^9 CFU/ml. Fluorescence analysis shows a 3.38–3.5 times enhanced signal. pH sensor presents a 2.14–3.08 times enhancement via the detection of cellar metabolite. Electrical measurements demonstrate an 8.8–26.7 times enhanced current. The proposed platform provides a new way of leveraging bio-inspired 3D printing and 2D materials for the development of sensing devices for biomedical applications.

1. Introduction

Bacteria-related diseases and complications, such as post-surgical infections, pneumonia, diarrhoea and urethritis, represent one of the major burdens of healthcare, globally affecting millions of patients each year (Zhang et al., 2015). As a result, real-time clinical monitoring and diagnostic systems have attracted extensive research interests. Commercially, the biosensors market is expected to grow steadily (Malhotra and Chaubey, 2003; Thusu, 2010) with a compound annual growth rate of 8.84% between 2017 and 2022 and reach 27 billion USD by 2022 (Salgarkar, 2017). The pressure from vulnerable patient groups such as the elderly and those with chronic diseases and comorbidities, as well as increasing incidents of Methicillin-resistant *Staphylococcus aureus* infection has called for effective sensing techniques in both clinical and environmental settings. Timely diagnosis of bacterial infections can significantly reduce complications and lower fatalities. There is a need for developing sensing techniques with lower detection limits, higher sensitivity, better selectivity and reproducibility for in situ, in vivo use. Current commercial biosensing processes used in hospitals to identify bacteria primarily rely on the conventional cell culturing/counting methods (Jung et al., 2008; Li et al., 2016) or fluorescent dye labelled probes (Biswas and Bandyopadhyaya, 2016), which react to specific bacteria strain. These require either a time-consuming culturing process or an expensive labelling procedure combined with complicated laser excitation/detection instruments.

There are, however, other signatures of bacteria that can be used for detection and identification, such as their effect on the conductivity on a 2D surface that they colonise and the pH value of their surrounding environment (Mannoor et al., 2012). Graphene, as a 2D material that possesses unique properties, such as high electronic and thermal conductivity, intrinsically high surface to volume ratio and chemical inertness – has been used to develop high sensitivity biosensors that are compatible with the current large-scale device fabrication processes (Li et al., 2017; Shao et al., 2010). They have the potential to provide an improved sensing performance, whilst reducing fabrication costs (Novoselov et al., 2005; Tian et al., 2014).

In this paper, the creation of the bio-inspired micro-structure for sensing is made possible using 2 photon polymerisation technologies (2PP). This is a versatile rapid-prototyping fabrication technique that has the advantages such as single-step fabrication (which can be adapted to be multi-step or multi-material) and three-dimensional design freedom. It can be used to create stand-alone devices (Kim et al., 2013) or to modify/integrate new features into existing devices (Thiele et al., 2016). There are many examples of bio-inspired microscale devices, including light-weight metamaterials mimicking bone structure (Bauer et al., 2014), swimming micro robots inspired by bacterial flagella (Tottori et al., 2012) and biocompatible adhesive surfaces with microstructures resembling a gecko's feet (Geim et al., 2003). Despite the fact that 2PP was originally targeted at the nano-photonics community, its value for biological and medical applications has been

* Corresponding author.
E-mail addresses: b.li@imperial.ac.uk (B. Li), s.anastasova-ivanova@imperial.ac.uk (S. Anastasova), g.z.yang@imperial.ac.uk (G.-Z. Yang).

https://doi.org/10.1016/j.bios.2018.09.087
Received 21 August 2018; Received in revised form 24 September 2018; Accepted 26 September 2018
Available online 27 September 2018

increasingly recognised. Examples of structures interacting directly with cells include microrobots for the targeted delivery of agents (Kim et al., 2013), cell scaffolds to study cell growth patterns (Accardo et al., 2018) and capsules for passive bacteria capture (Di Giacomo et al., 2017). There are also reports on the fabrication of electrochemical microfluidic devices using 3D printing methods (Damiati et al., 2017; Erkal et al., 2014; Gowers et al., 2015; Snowden et al., 2010). However, the combination of mechanical cell capturing, sorting and graphene-based sensing has not yet been investigated.

In this report, we demonstrate an enhanced bacteria sensor using the venous-valve-inspired structures. The proposed asymmetric 3D micro-structure rectifies the motion of *Escherichia coli* (*E. coli*) in certain directions and causes the increase of bacteria concentration in the designated chambers, in turn leading to the increase of the corresponding sensing signal. This mechanism can be utilized to lower the detection limit of a given bacterial sensor within the platform. The graphene electrical sensors were fabricated on SiO_2/Si substrate following the standard manipulating methods (Kim et al., 2009; Li et al., 2017). A novel 3D micro-structure was aligned and directly fabricated onto the graphene sensing area. To our knowledge, this is the first report of combining the bio-inspired 3D micro-structure with 2D material to enhance biosensing performance. As a proof-of-concept, this device is employed for the detection of a motile bacteria, E. coli, which provides a robust and reliable platform for potential use on surgical robotics to achieve a real-time detection of the bacteria caused infection. Fluorescence analysis presents the concentrating efficiency of 3.5 and 3.38 for high (10^9 cfu/ml) and low (10^3 cfu/ml) bacteria concentration respectively, while pH analysis shows 3.08 and 2.14 times concentrating efficiency respectively for the detection of same bacteria concentrations. Electrical measurements demonstrate a concentrating efficiency of 5.4 (current change) in cell culture medium, 8.8 (linear fitted slop) and 12.5 (current change) for the detection of different cell concentrations in motile buffer, respectively.

2. Material and methods

2.1. Reagents

Monolayer chemical vapour deposition (CVD) graphene on Cu foil was purchased from Graphene Supermarket (USA). Photoresist S1805, lift-off resist LoR 3B, the corresponding developer and remover 1165 were purchased from A-Gas Electronic Materials. IP-S resist was purchased from Nanoscribe. Chemicals, including pyrenebutyric acid N-hydroxysuccinimide ester (PANSE), Propylene glycol methyl ether acetate (PGMEA), phosphate-buffered saline tablet (PBS), Poly (methyl methacrylate) (PMMA) ammonium persulfate, glucose ($C_6H_{12}O_6$), ethylenediaminetetraacetic acid disodium salt dihydrate (EDTA, pH 7.0), Tween 20, Lysogeny broth (with/without agar) medium powder and sodium chloride (NaCl) at biochemical grade were purchased from Sigma Aldrich (UK).

2.2. Fabrication of graphene electronics and 3D micro-structure

A standard photolithography process was performed to fabricate the electrodes on a SiO_2/Si substrate. Positive photoresist S1805 was used as the masking layer for metal deposition and thermally evaporated Cr/Au were used as the adhesion and electrode materials. CVD graphene on Cu was wet transferred (Yan et al., 2017; Yu et al., 2008). Graphene on the back side of Cu was etched away by oxygen plasma (100 W, 2 min). The top layer graphene was spin-coated with PMMA (3000 r.p.m) and followed by a baking step (2 min, 200 °C). Cu foil is etched away using ammonium persulfate solution (15 g/L), followed by a thorough rinse in DI water. The floating graphene/PMMA was picked up using the pre-patterned SiO_2 substrate and post-baked (200 °C) to promote a stronger graphene/substrate adhesion. The PMMA layer was removed in warm acetone (60 °C, 30 min). The graphene and encapsulation SU-8 layer were patterned via standard photolithography (more details in Supplementary Information (SI)).

The venous-valve-inspired 3D micro-structure – was aligned and directly fabricated using Nanoscribe on graphene electronics. The writing power and the writing speed are chosen (12 mW, 10,000 μm/s) to avoid over-curing the IP-S resist. The development process was carried out by immersing the sample in PGMEA (30 min), followed by isopropyl alcohol rinsing (5 min).

2.3. Functionalisation of pH sensor and bacteria sensors

A further layer of electrochemically deposited Au nanoparticles was added using an aqueous solution of $HClO_4$ (0.1 M) and different concentrations of $HAuCl_4$ (1, 3, 5 and 7 mM), which minimised the initial voltage drift in measurements. Iridium oxide pH electrodes were achieved through electrochemical oxidation during potential cycling (0.6–1.1 V). The iridium oxide nanoparticle dispersion was from aqueous K_2IrCl_6 solution (3.0 mM), which was adjusted to pH 11 with aqueous NaOH (8 wt%) to obtain a yellow coloured solution (Zhao et al., 2011), which was then heated to 85 °C for 20 min. This solution was cooled to room temperature, then kept in an ice bath to obtain a blue coloured solution. This was then adjusted to pH 2 by rapidly adding HNO_3 (1 M) and stirred (40 min) until the solution became deep blue; it was then stored in a refrigerator (2–8 °C).

PANSE was used to functionalise graphene without introducing defects into the graphene lattice (Liu et al., 2013). A PANSE solution (2 mM) was prepared by adding PANSE powder (0.077 g) into methanol (100 ml) with shaking (2 h). The graphene electrode was immersed into this solution and sealed (1 h) at room temperature, followed by methanol rinsing to remove excess PANSE. The PANSE molecule consists of a four-benzene ring ends, which can be immobilised onto graphene via the non-covalent π-π bond, leaving the bioactive end free-standing in solution. Anti-*E. coli* (Abcam) solution (10 μl, 50 μg/ml) was added onto the surface of PANSE functionalised graphene and incubated overnight (4 °C). Then, the sensors were rinsed with PBS buffer and incubated with BSA (0.5 ml/ml) to block the free amino moieties. After 30 min, the sensors were rinsed with PBS buffer and stored at 4 °C. *E. coli* cell solution (from 10^1 cfu/ml to 10^9 cfu/ml) were prepared by dilution the fresh culture with motile buffer. The detection process was carried out by culturing cell solution (10 μl) on the sensor surface for 2 h to allow a strong antibody-antigen bonding.

2.4. Cell growth and counting

E. coli (MG1655) was cultured at 37 °C overnight in the LB (Miller) medium with a shaking speed of 240 r.p.m. The saturated growth medium was diluted by 100 times into fresh LB medium and cultured for another 4.5 h at same conditions. The growth medium was centrifuged at 2000 r.p.m. for 10 min to collect the cells. The pellet at the tube bottom was re-suspended by adding the motility buffer (10^{-2} M $C_6H_{12}O_6$, 10^{-4} M EDTA (pH 7.0), Tween 20 (0.2%), NaCl (76 mM) and PBS buffer (10 mM)). The different concentration of *E. coli* solutions were prepared by diluting the saturated growth medium. The concentration was evaluated by counting the colonies on the agar plates.

3. Results and discussion

3.1. Layout and working mechanism of bio-inspired graphene bacteria sensor

The structural layout and the working mechanism are presented in Fig. 1. The detailed fabrication procedures are presented in Fig. S1. Fig. 1(a) shows a longitudinal section of the venous valves in blood vessels. When the blood returns from distal vessels to the heart, the valves partially open. This prevents the backflow of blood in response to the manoeuvre or gravity (Karamichalis et al., 2017). With this in

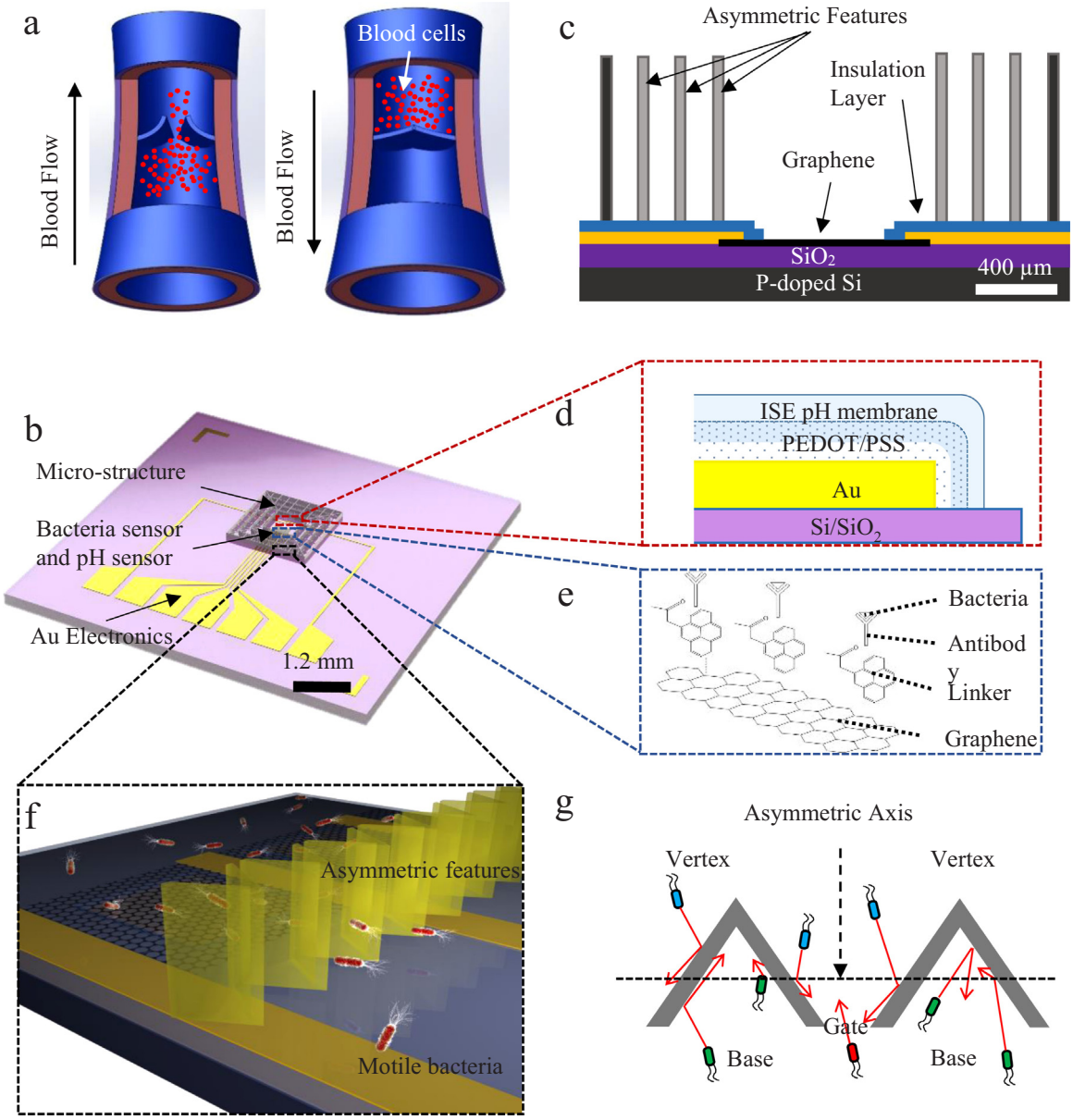

Fig. 1. Layout illustration of bio-inspired 3D micro-structure enhanced graphene sensor. (a) Schematic diagram of the venous valves in blood vein. (b) 3D view of the sensor on SiO_2/Si substrate. (c) Cross-section of the graphene bacteria sensor. (d) Cross-section of pH sensor and (e) chemical functionalisation of bacteria sensor. (f) 3D view of concentrating mechanism. (g) Top view of the asymmetric features and 2D concentrating mechanism.

mind, a 3D micro-structure enhanced graphene bacteria sensor has been designed – that applies the use of directional valves to guide bacteria towards a sensor. The sensor's Au electrodes are pre-fabricated on SiO_2/Si substrate and the graphene channel connects the source and drain. Then, the centre of 3D micro-structure is aligned with the centre of graphene sensors on SiO_2/Si substrate and fabricated using 2PP, as shown in Fig. 1(b).

Fig. 1(c) shows a cross section of the graphene bacteria sensor. An insulating layer of SU-8 is spin-coated to encapsulate the electronic device, with open windows to expose only the functionalised graphene for sensing purposes. The 3D micro-structure consists of three concentric layers of walls with asymmetric valve features (light grey) and one sealed wall (darker grey) to ensure that the number of bacteria in each experiment is kept constant. The proposed bacteria sensors and pH sensor are presented in Fig. 1(d) and (e). In this sensing system, the surface of the graphene windows are functionalised with PANSE and bacteria antibodies, as shown in Fig. 1(e). The working mechanism of the graphene sensor is that when bacteria binds onto the graphene surface, a change in the charge carrier density results, in turn leading to a resistance change in graphene channel (Ahn et al., 2010). A pH sensor (shown in Fig. 1(d)), which consists of a conductive layer and ISE membrane, is integrated within the central area and used to cross check the enhanced performance of graphene bacteria sensors.

Fig. 1(f) and (g) demonstrate the mechanism of bacteria concentrating in the central area. The initial distribution of bacteria is random and uniform, which means the concentration of bacteria on the either side of the wall is equal. When the bacteria solution is added to this asymmetric 3D structure, for individual bacterium, it induces a random swimming with a linear length of about 50 µm. The mechanism of the bacteria trapping was first explained by the self-propelling motion of *E. coli* (Galajda et al., 2008). In summary, when encountering the wall from the vertex side (as labelled in Fig. 1(g)), a single bacterium (illustrated as blue rods) could keep moving towards the funnel or swim away from it. Therefore, it is expected to have a 50% probability of sliding along the wall and through the funnel. However, when approaching the wall from the base side, a bacterium is most likely to be

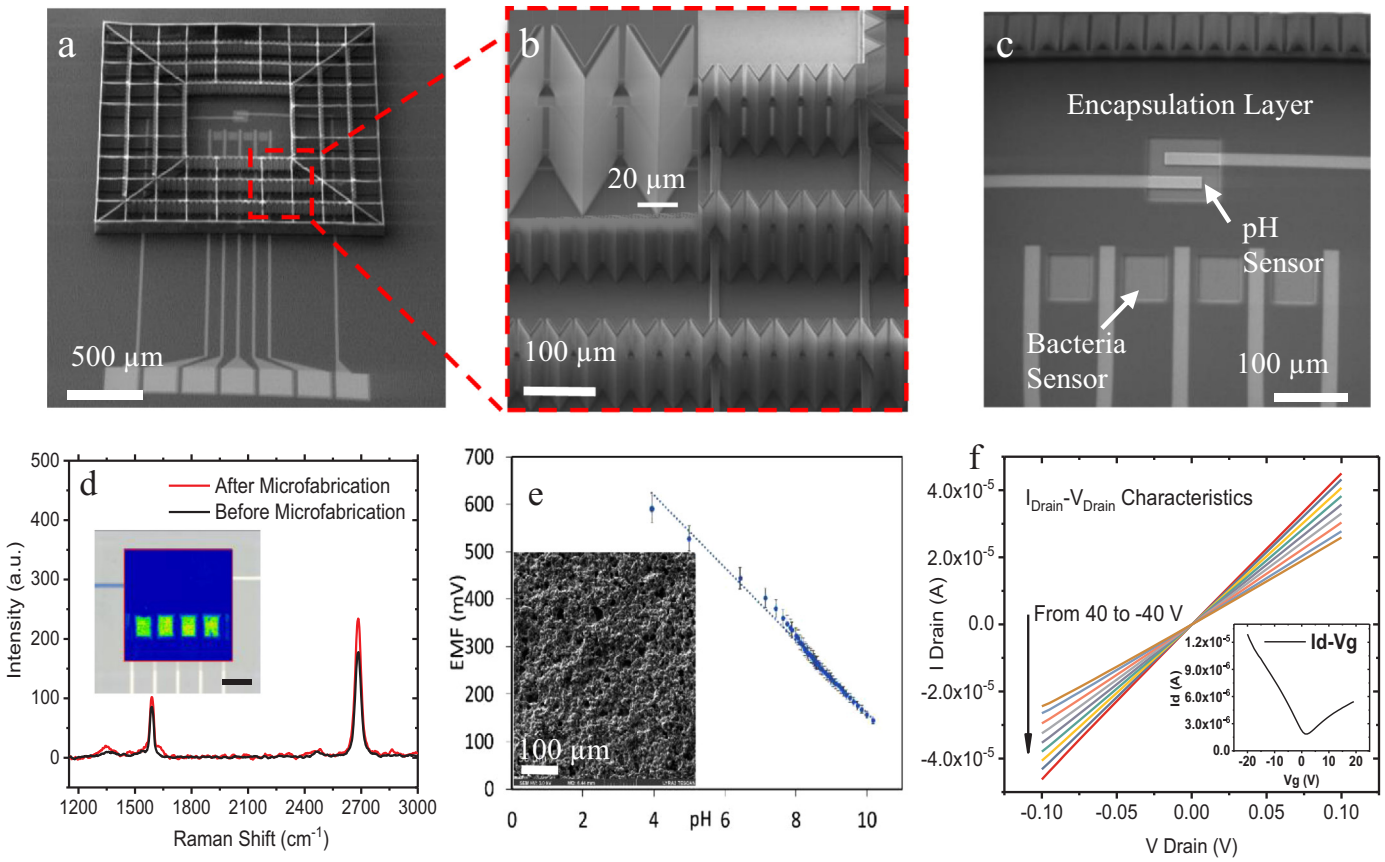

Fig. 2. Fabrication and validation of the sensor component. (a) SEM over view of the entire 3D structure enhanced graphene sensor and (b) the asymmetric features. (c) SEM image of the graphene windows (x4) and pH sensing components. (d) Raman characterisation of graphene sensing area. Inset: G band mapping of graphene channel, scale bar 80 µm. (e) Calibration of pH sensor and SEM image of pH membrane. (f). I_d-V_d characteristics of encapsulated graphene device. Inset: I_d-V_g characteristic of pristine graphene.

diverted away from the funnel and, therefore, it becomes trapped on one side of the wall (shown as green rods). The only exception among them are the few bacteria that swim towards the gate directly (shown as a red rod) to make it backwards through the wall of valves. However, as the length of the gate is much smaller than the vertex-to-vertex length, the majority of bacteria tend to move in the vertex-to-base direction, leading to a higher bacteria concentration at the central area of the micro-structure, allowing effective signal amplification. The concentrating efficiency is defined as:

$$E = \frac{N1}{N2} \quad (1)$$

where N1 and N2 are defined as the number or the signal intensity of bacteria in the inner block and the outer block, respectively.

3.2. Characterisation of 3D micro-structure enhanced graphene bacteria sensor

The characterisation of the graphene sensor and a detailed analysis of its individual components are presented in Fig. 2. Fig. 2(a) shows an overview of the entire 3D structure-enhanced graphene bacteria sensor. The final device has a vertical height of 110 µm, with three independent components; namely a 3D micro-structure, a pH sensor and graphene electronics. The solid outer wall of 3D micro-structure is designed to ensure the number of bacteria inside is constant throughout the experiment, and that only the relative concentrations of the three blocks changes over time. Three layers of filter walls (with the most central one of 600 × 600 µm and separation of 200 µm), which consist of asymmetric features, function as passive valves to allow bacteria to have a higher probability of moving from the outer blocks to inner ones, and not the other way around (shown in Fig. 2(b)). The gate width between the two asymmetric valve-like features is designed to be 4 µm (shown in the inset of Fig. 2(b)), which is larger than the body length of the *E. coli* (0.5–2 µm) used in this work. The gate width allows all bacteria to pass through the gate, regardless of orientation. The pH sensor and graphene-based bacteria sensor are positioned in the centre of the 3D micro-structure, as shown in Fig. 2(c). A graphene channel is patterned to bridge over the four Au electrodes. The graphene windows (indicated by arrow) are chemically functionalised and used as bacteria sensors. The remaining graphene and electronics outside of the window are protected by the insulating layer (as labelled in Fig. 2(c)).

Raman spectroscopy was used to characterise the quality of the pristine graphene. A representative spectrum has been taken before and after the microfabrication and 3D printing, as shown in Fig. 2(d). The D/G band ratio shows a minor increase from 0.11 to 0.17 and G/2D band ratio decreases from 0.51 to 0.48, indicating the pristine graphene is slightly doped by the unavoidable resist residues after the microfabrication process (Tien et al., 2016). A mapping of G band position is shown as the inset to prove the continuity of graphene. Calibration of the pH sensors and the scanning electron microscope (SEM) of the sensing electrodeposited IrO_x membrane is shown in Fig. 2(e). The sensor shows super-Nernstian response in a sensitivity of −76.4 mV/unit and a linear working range between pH 4–10 at 25 °C, indicating a sensing capability in a limited space with distinct responding potentials at various pH levels.

The electrical characteristics of the pristine graphene and resist-encapsulated device are presented in Fig. 2(f). A Dirac point at 3 V could be seen from the I_{drain}-V_{gate} characterisation (Fig. 2(f) inset), indicating the good quality of pristine graphene channel after the

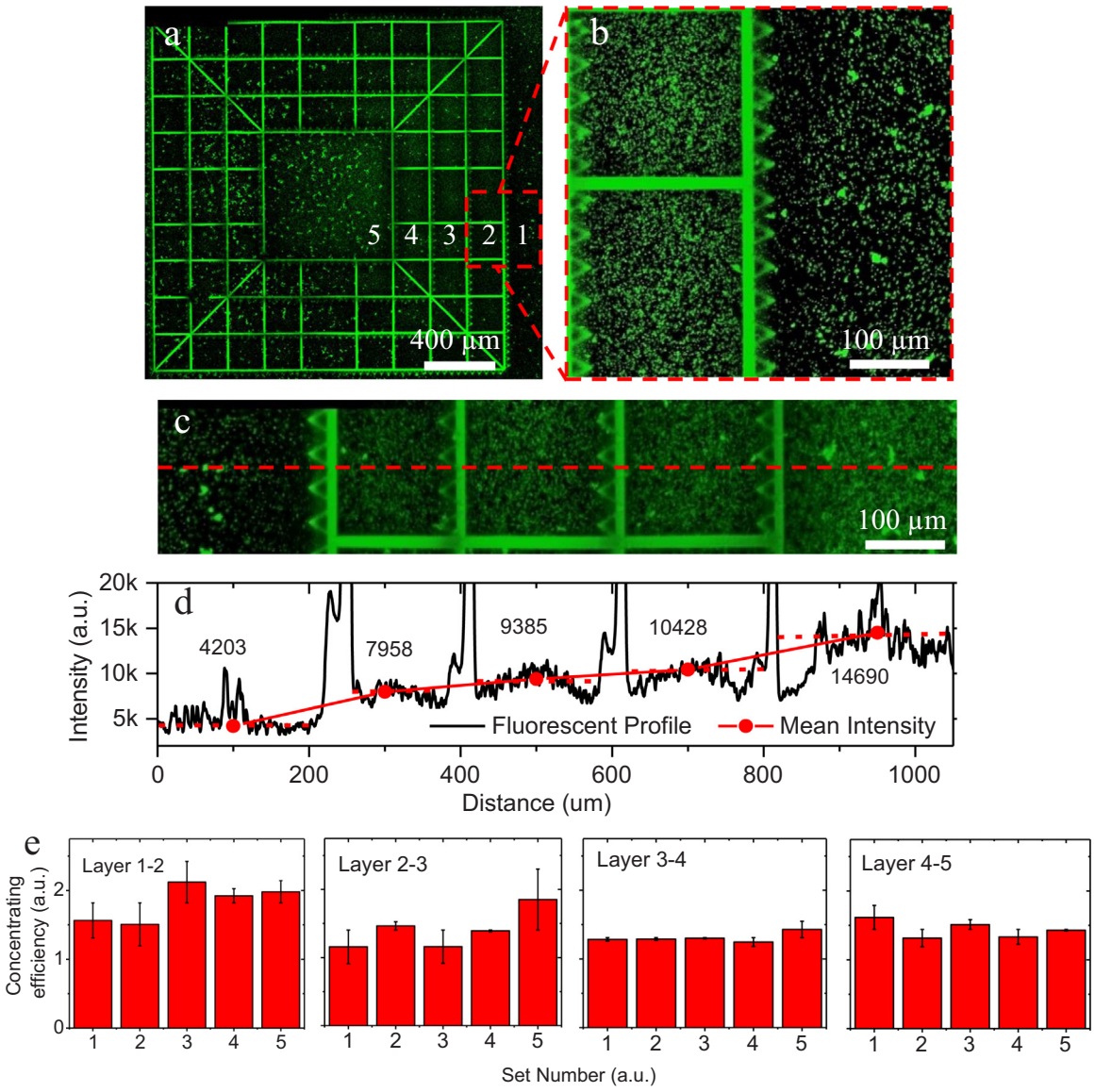

Fig. 3. The distribution analysis of fluorescent bacteria in the 3D micro-structure (bacteria concentration is 10^9 cfu/ml). (a) Overview the fluorescent bacteria in micro concentrator. (b) Local distribution contrast inside (right) and outside (left) of the wall. Larger dots are cell clusters. (c) Wall arrays act as a pump to concentrate cells from one reservoir into another. (d) Fluorescence line profile (black) and the average intensity (red, excludes signals from 3D structure). (e) Statistical concentrating efficiency between the two adjacent blocks (five sets independent measurements).

transfer/pattern process. After the fabrication of the encapsulation layer, the I_{darin}-V_{drain} characteristics show a trend of increased conductivity, when the source-drain voltage is scanned from 40 V to −40 V. This indicates that the graphene-based sensor has been heavily doped (Dong et al., 2009) and will operate in the p-type region of graphene for the detection of bacteria cells.

3.3. Fluorescence analysis of bacteria in 3D micro-structure

The fluorescence analysis of the concentrating behaviour of the motile bacteria within the 3D micro-structure is presented in Fig. 3. The 3D micro-structure, which releases a fluorescent signal at 520 nm, provides a sharp view of the block boundaries. Each individual green dot (due to intracellular fluorescent protein) represents one *E. coli* cell. The fluorescent signal in the central square is generally higher than that of the outer blocks, as shown in Fig. 3(a). Fig. 3(b) shows a zoomed in image of the bacteria distribution on both sides of one asymmetric wall. The fluorescence signal from the inner block is 1.9 times stronger than that of the outer block, indicating an effective concentrating performance. Fig. 3(c) shows an analysis of the bacteria distribution across the entire 3D micro-structure, which acts as a passive pump driving bacteria from the outer blocks towards the central square. The corresponding fluorescence line profile of Fig. 3(c) and the average fluorescence intensity (excludes signals from 3D structure) is shows as back and red lines in Fig. 3(d), respectively. It presents an average concentrating efficiency of 1.4 for single wall and the overall concentrating efficiency of 3.5 for the whole device (calculated as intensity ratio 14690/4203). The statistical analysis is carried out by measuring the intensity of florescence signal in 5 different areas in every two adjacent blocks. As shown in Fig. 3(e), the concentrating efficiencies are calculated to be 1.82, 1.41, 1.31 and 1.44 for each wall from outside to centre. This concentrating effect works at both high and low bacteria concentrations. An analysis of bacteria distribution at a lower concentration (10^3 cfu/ml) and the control experiment without the 3D micro-structure are shown in Fig. S3.

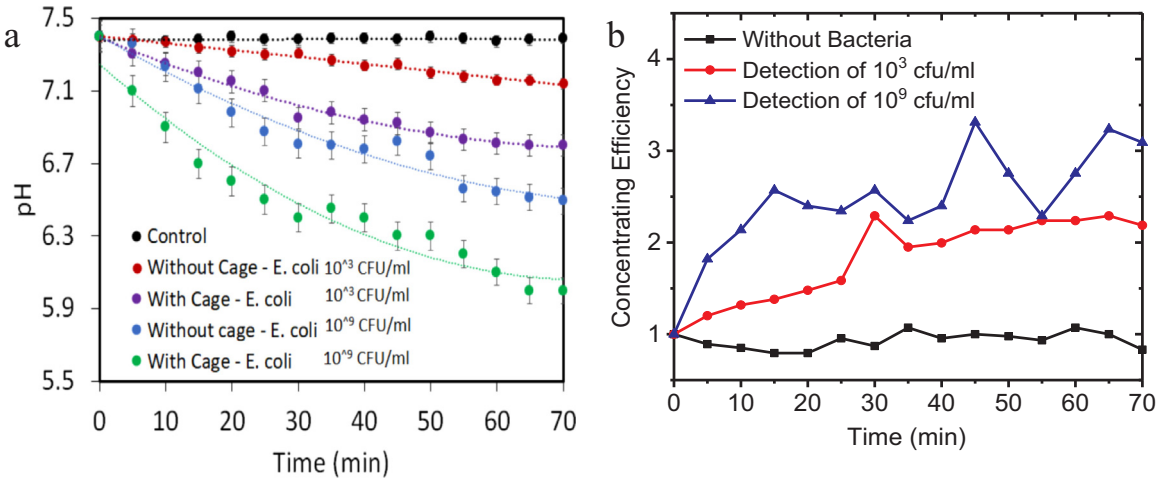

Fig. 4. pH analysis of 3D micro-structure enhanced graphene bacteria sensor (a) Comparison of the response to pH from bacteria culture without and with a micro-structure towards the detection of 10^3 and 10^9 cfu/ml concentration. (b) Concentrating efficiency vs time for the detection of 10^3 and 10^9 cfu/ml *E. coli*. Detection towards blank buffer is shown as control.

3.4. Enhanced pH sensing in 3D micro-structure

The Enhanced pH sensing performance has been carried out using a thin film pH sensor embedded in the 3D micro-structure, which is used as a cross-checking method for bacteria cell sensing. A comparison of the results is presented in Fig. 4. Based on Nernst equation pH unit change would cause a difference of 59 mV. In our case where IrOx is acquired by electroplating the hydrous form and oxide formation is a bit more complex which depends on the deposition conditions (Eq. (1)). The sensitivity of the pH sensor is 76.4 mV/unit E. coli cell.

$$2[IrO_2(OH)_2{\cdot}2H_2O]^{2-} + 3H^+ + 2e^- \leftrightarrow [Ir_2O_3(OH)_3{\cdot}3H_2O]^{3-} + 3H_2O \quad (2)$$

The pH values obtained without the 3D micro-structure at two different concentrations are plotted in red and blue lines, and those values obtained from the devices with 3D micro-structures are plotted in purple and green for the detection of 10^3 cfu/ml and 10^9 cfu/ml bacteria respectively, as shown in Fig. 4(a). Devices with 3D micro-structure are also measured in blank solution (without bacteria as control) to ensure the change of pH is caused by the accumulation of bacteria (black line). From the graphs, for a given concentration, the devices with a 3D micro-structure surrounding the sensing region result in a much lower pH than without the micro-structure. The concentrating efficiency increases quickly for the first 30 min and gently afterwards, reaching a value of 2.14 and 3.08 for the detection of 10^3 cfu/ml and 10^9 cfu/ml bacteria at 70 min (as shown in Fig. 4(b)). This is explained by the fact that *E. coli* cells ferment sugar molecules, thereby increasing the acidity of the surroundings and resulting in a lower pH (Shaibani et al., 2016). This is consistent with the fluorescence analysis in Fig. 3, which proves the concentrating efficiency of the venous-valve-inspired 3D micro-structure.

3.5. Enhanced bacteria sensing performance

Electrical characterisation has been performed to evaluate the sensing performance for the detection of *E. coli* cells in Fig. 5. Fig. 5(a) shows SEM images of the control experiment of the cells immobilised on functionalised and non-functionalised graphene surface. The darker graphene surface (upper-left of red dashed line), which has been successively functionalised by the PANSE and anti-*E. coli*, presents strong adhension to *E. coli* (700 cfu/sensing window, shown in Fig. S3) after dipping in the 10^9 cfu/ml cell solution, whilst there is no observation of *E. coli* cells immobilised on the non-functionalised graphene surface. The immobilisation efficiency observed in this work is lower than previous reports (Suo et al., 2009). This may be attributed to the high mobility of the specific strain of bacteria chosen for this study, which is more suitable for passing through the asymmetric 3D micro-structure and reaching equilibrium in a shorter timespan. As a result, however, they are more difficult to immobilise using the antibody.

Fig. 5(b) presents the change of I_{ds}-V_{ds} characteristics after each functionalisation step and against the detection of 10^6 cfu/ml *E. coli*. The conductance of the linker/antibody/BSA functionalised surface increases from 2.40×10^{-6} A to 2.91×10^{-6} A with the attachment of negatively charged *E. coli* cells onto the graphene sensing window. As the graphene is operated at the p-type region (demonstrated in Fig. 2(f)), the increase of electrical conductance is attributed to the increased hole doping level, which is due to the negatively charged cell surface protein at a pH of 7.2 (Mohanty and Berry, 2008). The current change in cell culture versus timeline is shown in Fig. 5(c). Electrical current slightly increases from 5.37×10^{-6} A to 5.56×10^{-6} A in the first 10 min (indicated by the black arrow), and then decreases slowly to 3.54×10^{-6} A in the next 80 min on the device without the 3D micro-structure. On the device with the 3D micro-structure, the current shows a similar change trend, but with a 5.4 times higher peak signal of 2.1×10^{-5} A at 30 min, (indicated by a red dashed line). The increase in current at the beginning is attributed to the negatively charged cell surface as demonstrated in Fig. 5(b), whilst the following current drop over time is attributed to the accumulation of acid produced by the live cells. As shown in Fig. 5(d), the current decreases with the decrease of pH values, which is in accordance with a previous report (Huang et al., 2011).

Fig. 5(e) shows the current change against the detection of different cell concentrations ranging from 10^1 to 10^9 cfu/ml. By adding the 3D micro-structure on top of the graphene sensors, the linear fitting of the curves changes from $y = 8.86*10^{-8}x + 3.60*10^{-8}$ to $y = 7.81*10^{-7}x + 1.50*10^{-6}$, presenting an 8.8 times increase in the slopes. The current changes also shows on average a 12.5 times increase (observed range 8.8–26.7 times increase at different concentrations), indicating the effective concentrating function of the 3D micro-structure. Fig. 5(f) shows one presentative detection run against the blank reference sample (PBS buffer) and the inset shows a summary of 7 independent measurements. The standard deviation of noise (σ) can be extracted as 2.64×10^{-8} A. By taking the 3σ (three times signal to noise ratio), the limit of detection is calculated to be 7.92×10^{-8} A for a single device, which equals to the detection of 10° cfu/ml cells.

However, it is noted that the higher cell concentration will lead to a larger number of non-specifically attached cells on the graphene sensing surface. In addition, as graphene can be easily damaged and doped

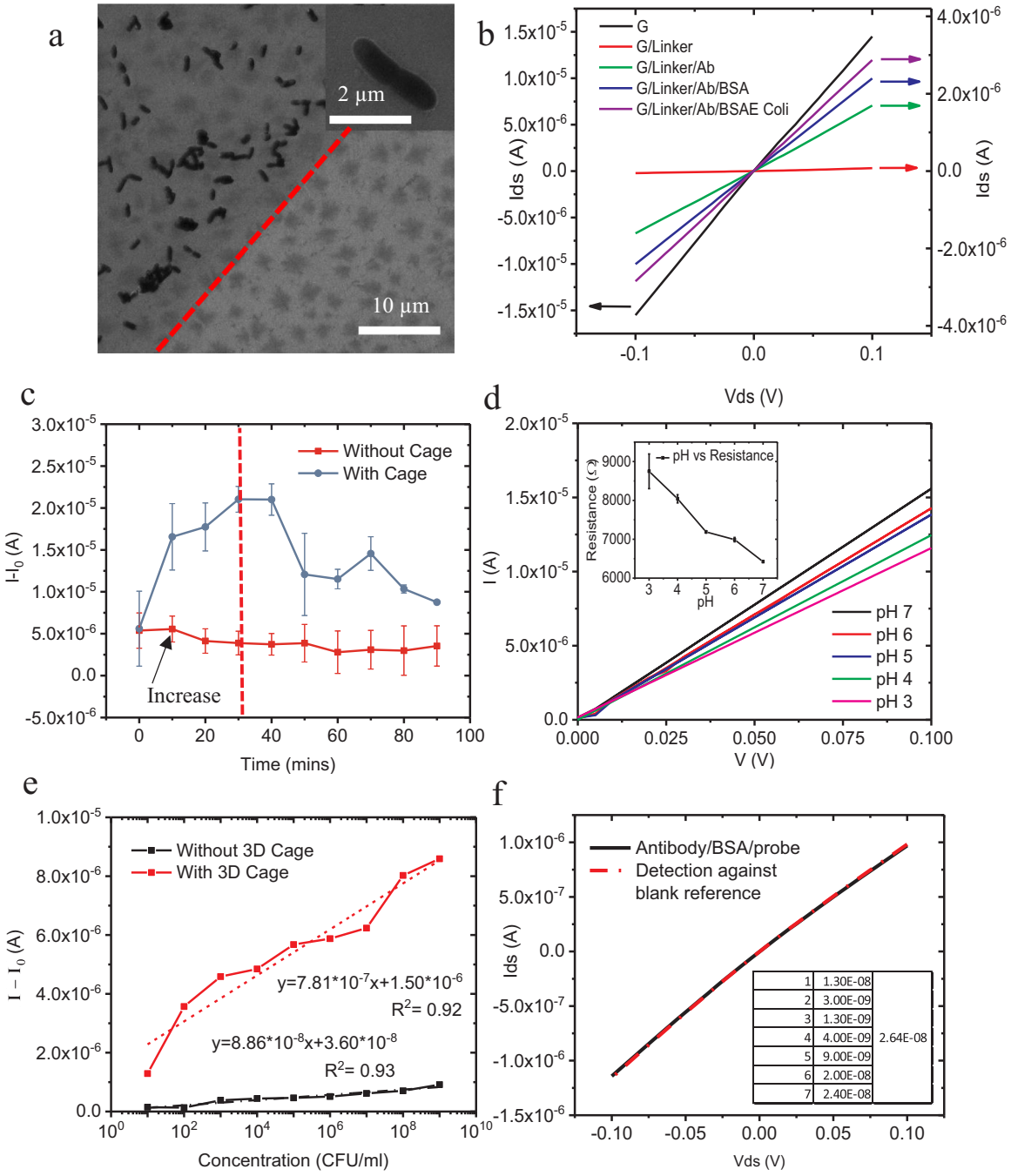

Fig. 5. Electrical analysis of 3D micro-structure enhanced bacteria sensing performance. (a) Control experiment of cell bonding on the functionalised and the non-functionalised graphene. Inset: individual *E. coli* immobilised on the functionalised graphene. (b) Transfer curves of one graphene sensing window after functionalization. (c) Electrical current vs time for the detection of *E. coli* in culture medium. (d) Electrical signal vs standard pH references. (e) Electrical detection of different cell concentrations from the devices with/without the 3D micro-structures. (f) Determination of LoD against blank references. Inset: n = 7 measurements.

during the fabrication and functionalisation process, the signal drift is a common issue in biosensing (Sotiropoulou et al., 2003). Therefore, the concentrating efficiency in practice will be lower than those value observed above.

4. Conclusions

We have proposed and implemented a venous-valve-inspired 3D micro-structure to enhance the graphene sensor performance for the detection of motile bacteria. The proposed mechanism relies on the asymmetry of the 3D printed structure, which allows the motile cell swim readily from outside the trap towards the centre, but not vice versa. The concentrating effect has been confirmed by fluorescence analysis, which shows a 3.38–3.5 times enhancement. The pH sensors embedded in the centre of the trap presents an enhancement of 2.14–3.08 times. Electrical measurements demonstrate the concentrating efficiencies of 5.4 in a cell culture medium, 8.8 (linear fitted slope) in PBS and 8.8–26.7 for the detection of different cell concentrations. This proof-of-concept platform offers a promising route for combining cutting-edge 3D printing technology, bio-inspired design and 2D materials together to achieve a high-performance biosensor for surgical applications.

Acknowledgement

This work was financially supported by the Engineering and Physical Sciences Research Council (EPSRC), United Kingdom [EP/L014149/1, Smart Sensing for Surgery], [EP/P012779, Micro-Robotics for Surgery] and Imperial College Healthcare NHS Trust-BRC, United Kingdom [WSSS_P69945].

We thank Dr. Tom Ellis group for providing the motile *E. Coli*.

Appendix A. Supporting information

Supplementary data associated with this article can be found in the online version at doi:10.1016/j.bios.2018.09.087.

References

Accardo, A., Blatché, M.-C., Courson, R., Loubinoux, I., Vieu, C., Malaquin, L., 2018. Mater. Today 21 (3), 315–316.
Ahn, J.-H., Choi, S.-J., Han, J.-W., Park, T.J., Lee, S.Y., Choi, Y.-K., 2010. Nano Lett. 10 (8), 2934–2938.
Bauer, J., Hengsbach, S., Tesari, I., Schwaiger, R., Kraft, O., 2014. Proc. Natl. Acad. Sci. USA 111 (7), 2453–2458.
Biswas, P., Bandyopadhyaya, R., 2016. Water Res. 100, 105–115.
Damiati, S., Küpcü, S., Peacock, M., Eilenberger, C., Zamzami, M., Qadri, I., Choudhry, H., Sleytr, U.B., Schuster, B., 2017. Biosens. Bioelectron. 94, 500–506.
Di Giacomo, R., Krödel, S., Maresca, B., Benzoni, P., Rusconi, R., Stocker, R., Daraio, C., 2017. Sci. Rep.-UK 7, 45897.
Dong, X., Fu, D., Fang, W., Shi, Y., Chen, P., Li, L.J., 2009. Small 5 (12), 1422–1426.
Erkal, J.L., Selimovic, A., Gross, B.C., Lockwood, S.Y., Walton, E.L., McNamara, S., Martin, R.S., Spence, D.M., 2014. Lab Chip 14 (12), 2023–2032.
Galajda, P., Keymer, J., Dalland, J., Park, S., Kou, S., Austin, R., 2008. J. Mod. Opt. 55 (19–20), 3413–3422.
Geim, A.K., Dubonos, S., Grigorieva, I., Novoselov, K., Zhukov, A., Shapoval, S.Y., 2003. Nat. Mater. 2 (7), 461.
Gowers, S.A.N., Curto, V.F., Seneci, C.A., Wang, C., Anastasova, S., Vadgama, P., Yang, G.-Z., Boutelle, M.G., 2015. Anal. Chem. 87 (15), 7763–7770.
Huang, Y., Dong, X., Liu, Y., Li, L.-J., Chen, P., 2011. J. Mater. Chem. 21 (33), 12358–12362.
Jung, W.K., Koo, H.C., Kim, K.W., Shin, S., Kim, S.H., Park, Y.H., 2008. Appl. Environ. Microb. 74 (7), 2171–2178.
Karamichalis, J.M., Aguib, H., Anastasopulos, A., Yacoub, M., 2017. J. Thorac. Cardiov Surg. 153 (2), 396–398.
Kim, K.S., Zhao, Y., Jang, H., Lee, S.Y., Kim, J.M., Kim, K.S., Ahn, J.-H., Kim, P., Choi, J.-Y., Hong, B.H., 2009. Nature 457 (7230), 706.
Kim, S., Qiu, F., Kim, S., Ghanbari, A., Moon, C., Zhang, L., Nelson, B.J., Choi, H., 2013. Adv. Mater. 25 (41), 5863–5868.
Li, B., Pan, G., Suhail, A., Islam, K., Avent, N., Davey, P., 2017. Carbon 118, 43–49.
Li, J., Ahn, J., Liu, D., Chen, S., Ye, X., Ding, T., 2016. Appl. Environ. Microb. 82 (6) (AEM. 03080-03015).
Liu, F., Kim, Y.H., Cheon, D.S., Seo, T.S., 2013. Sens. Actuators B-Chem. 186, 252–257.
Malhotra, B.D., Chaubey, A., 2003. Sens. Actuator B-Chem. 91 (1–3), 117–127.
Mannoor, M.S., Tao, H., Clayton, J.D., Sengupta, A., Kaplan, D.L., Naik, R.R., Verma, N., Omenetto, F.G., McAlpine, M.C., 2012. Nat. Commun. 3, 763.
Mohanty, N., Berry, V., 2008. Nano Lett. 8 (12), 4469–4476.
Novoselov, K.S., Jiang, D., Schedin, F., Booth, T.J., Khotkevich, V.V., Morozov, S.V., Geim, A.K., 2005. Proc. Natl. Acad. Sci. USA 102 (30), 10451–10453.
Salgarkar, R., 2017. Biosensors Market worth 27.06 Billion USD by 2022. Markets and Markets. URL: ⟨https://www.marketsandmarkets.com/PressReleases/biosensors.asp⟩.
Shaibani, P.M., Jiang, K., Haghighat, G., Hassanpourfard, M., Etayash, H., Naicker, S., Thundat, T., 2016. Sens. Actuators B-Chem. 226, 176–183.
Shao, Y., Wang, J., Wu, H., Liu, J., Aksay, I.A., Lin, Y., 2010. Electroanalysis 22 (10), 1027–1036.
Snowden, M.E., King, P.H., Covington, J.A., Macpherson, J.V., Unwin, P.R., 2010. Anal. Chem. 82 (8), 3124–3131.
Sotiropoulou, S., Gavalas, V., Vamvakaki, V., Chaniotakis, N., 2003. Biosens. Bioelectron. 18 (2–3), 211–215.
Suo, Z., Yang, X., Avci, R., Deliorman, M., Rugheimer, P., Pascual, D.W., Idzerda, Y., 2009. Anal. Chem. 81 (18), 7571–7578.
Thiele, S., Gissibl, T., Giessen, H., Herkommer, A.M., 2016. Opt. Lett. 41 (13), 3029–3032.
Thusu, R., 2010. Strong growth predicted for biosensors market. Sensors (URL). ⟨https://www.sensorsmag.com/components/strong-growth-predicted-for-biosensors-market⟩.
Tian, J., Yuan, P.-X., Shan, D., Ding, S.-N., Zhang, G.-Y., Zhang, X.-J., 2014. Anal. Biochem. 460, 16–21.
Tien, D.H., Park, J.-Y., Kim, K.B., Lee, N., Seo, Y., 2016. Sci. Rep. 6, 25050.
Tottori, S., Zhang, L., Qiu, F., Krawczyk, K.K., Franco-Obregón, A., Nelson, B.J., 2012. Adv. Mater. 24 (6), 811–816.
Yan, S., Zhu, X., Frandsen, L.H., Xiao, S., Mortensen, N.A., Dong, J., Ding, Y., 2017. Nat. Commun. 8, 14411–14418.
Yu, Q., Lian, J., Siriponglert, S., Li, H., Chen, Y.P., Pei, S.-S., 2008. Appl. Phys. Lett. 93 (11), 113103.
Zhang, Y.-J., Li, S., Gan, R.-Y., Zhou, T., Xu, D.-P., Li, H.-B., 2015. Int J. Mol. Sci. 16 (4), 7493–7519.
Zhao, Y., Hernandez-Pagan, E.A., Vargas-Barbosa, N.M., Dysart, J.L., Mallouk, T.E., 2011. J. Phys. Chem. Lett. 2 (5), 402–406.